

Optical nonlinearity in Ar and N₂ near the ionization threshold

J. K. Wahlstrand, Y.-H. Cheng, and H. M. Milchberg
*Institute for Research in Electronics and Applied Physics,
University of Maryland, College Park, MD 20742 USA*

We directly measure the nonlinear refractive index in argon and nitrogen in a thin gas target at laser intensities near the ionization threshold. No instantaneous negative nonlinear refractive index is observed, nor is saturation, in contrast with a previous measurement [Loriot *et al.*, *Opt. Express* **17**, 13429 (2009)] and calculations [Brée *et al.*, *Phys. Rev. Lett.* **106**, 183902 (2011)]. In addition, we are able to cleanly separate the electronic and rotational components of the nonlinear response in nitrogen. In both Ar and N₂, we observe the peak instantaneous index response scale linearly with the laser intensity until the point of ionization, whereupon it turns abruptly negative and \sim constant, consistent with plasma generation.

The optical Kerr effect, which describes the intensity-dependent refractive index experienced by an optical pulse in a transparent medium, plays an important role in phenomena from nonlinear propagation in optical fibers [1] to mode-locking in pulsed lasers [2] to filamentary propagation in condensed media and the atmosphere [3]. A recent transient birefringence measurement [4] on the components of air was purported to show that the optical Kerr effect saturates and then becomes negative for intensities greater than 26 TW/cm². This claim of a strong higher-order Kerr effect (HOKE), with a crossover from positive to negative nonlinear index at intensities well below the ionization threshold, has inspired theoretical works predicting plasma-free light filamentation [5] and exotic new effects in light propagation [6]. If it were true, this would overturn the picture most have of the mechanism behind long-range filamentary propagation of intense ultrashort pulses – as arising from a dynamic balance between self-focusing due to the optical Kerr effect and defocusing due to the plasma generated by ionization.

Subsequent experimental studies of light filaments [7–10] have not supported the role of HOKE in filamentation, with one exception [11]. Third- and fifth-harmonic generation has also been studied as a test of HOKE [12, 13]. A physical mechanism for HOKE has been proposed based on the nonlinear response near the threshold of ionization [14, 15], but these theories predict saturation of the Kerr effect at significantly higher intensities than observed in [4]. What is missing from this debate is a direct measurement of the nonlinearity that corroborates or refutes the intensity dependence observed by Loriot *et al.* Here, we describe a direct measurement of the high-intensity optical nonlinearity in Ar and N₂ using spectral interferometry. We find no significant saturation and no negative *instantaneous* nonlinear phase, indicating serious flaws in the experiment that started this controversy [4].

The technique we use is supercontinuum single-shot spectral interferometry (SSSI) [16]. It provides a single-shot measurement of the transverse space- and time-dependent phase shift of a chirped probe pulse due to

cross-phase modulation induced by a short pump pulse. The time resolution is given by the probe bandwidth (in this experiment \sim 15 fs) and the transverse spatial resolution here is 3 μ m. We note that the technique in [4] is a non-spatially resolved multi-shot technique limited in time resolution by the probe duration of \sim 100 fs. The results of [4] essentially represent a space and time convolution. By changing the relative polarization of the pump and probe pulses, we can measure parallel and perpendicular components of the nonlinear index independently. Note that Loriot *et al.* measured the transient birefringence and needed to use the tensorial symmetry of the nonlinear optical susceptibilities $\chi^{(5)}$, $\chi^{(7)}$, etc. to infer the HOKE coefficients [4, 17]. Previously, SSSI was used with 110 fs pump pulses to study the nonlinear response of the components of air [18], and no sign reversal of the nonlinear index was observed up to intensities where significant ionization occurs. However, the use of a gas cell can complicate the interpretation of the experiment when the response is highly nonlinear [19]. Also, at the high pressures used ($>$ 3 atm) plasma-induced refraction limits the peak intensity. Here, we measure the nonlinear response of argon and nitrogen using SSSI with a 38 fs pump pulse and a 2 mm thick gas target.

A diagram of the experimental setup and example data are shown in Fig. 1. Detailed descriptions of the SSSI technique have been given previously [16, 18]. The laser is a 1 kHz repetition rate Ti:sapphire amplifier producing 38 fs full width at half maximum (FWHM), 3.5 mJ pulses centered at 800 nm. Roughly 700 μ J of the laser output is used to generate supercontinuum (SC) covering 640-720 nm in a gas cell (not shown) filled with 1-2 atm of Ar; the fundamental is rejected using a dichroic mirror. The SC is linearly polarized. Probe and reference SC pulses, separated by 1.4 ps, are generated using a Michelson interferometer and chirped so that the group delay dispersion (GDD) is 1950 fs². The SC beam is spatially filtered with a 100 μ m pinhole. The pump power is attenuated using waveplates and thin film polarizers so that the pulse energy is continuously adjustable from 5-100 μ J. A $\lambda/2$ waveplate in the pump path allows rotation of the pump polarization. The pump beam is then

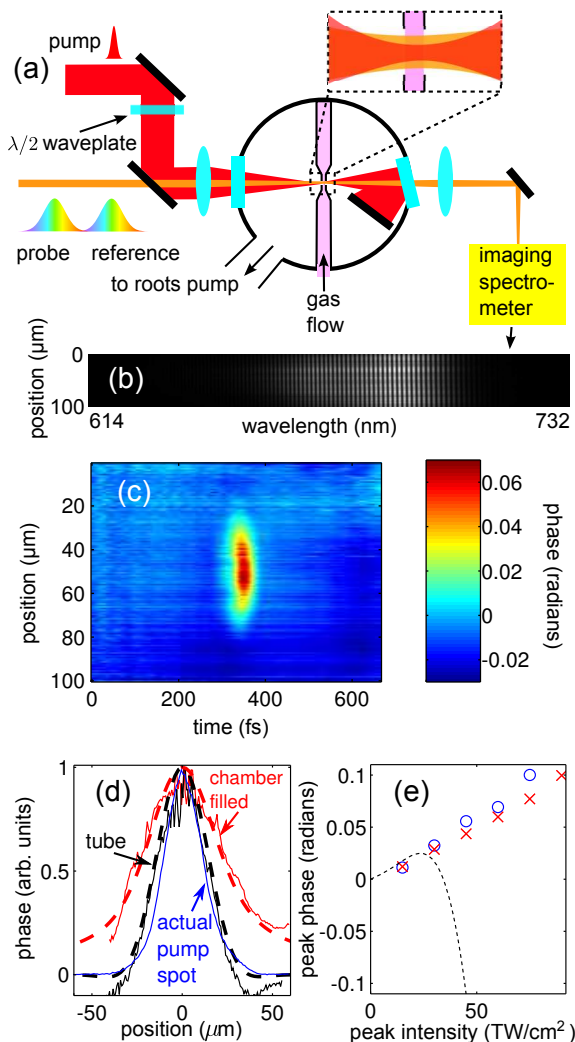


FIG. 1: (color online) Experimental apparatus and results. (a) Simplified experimental setup diagram showing the pump and SC pulses focused on a flowing gas target in a vacuum chamber. (b) An example interferogram. (c) Extracted map of phase versus time t and transverse dimension x using Ar at $I_{\text{peak}} = 60 \text{ TW/cm}^2$, extracted using the SSSI algorithm [16]. (d) A lineout of the pump spot at $t = t_{\text{pump}}$, comparing the signal using the drilled flow tube to the signal with a backfilled chamber. The true pump spot is also shown for comparison. The dashed lines show the results of propagation simulations [19] for the case of a backfilled chamber and for an interaction length of 2 mm. (e) The measured peak phase shift for $\mathbf{E}_{\text{pump}} \parallel \mathbf{E}_{\text{probe}}$ as a function of peak intensity for Ar (\times) and N_2 (\circ). The calculated peak phase shift in Ar using the HOKE coefficients given in [4] is shown as a dashed line.

expanded with a telescope. The pump and SC are combined using a dichroic mirror; at this point the pump beam is about 5 times wider than the probe beam.

A well-defined interaction length, ideally comparable or shorter than the Rayleigh range of the pump beam, minimizes spatial and temporal distortions in the measured phase shifts due to axial variation in the pump

intensity [19]. To approach this, we use a thin gas target inside a vacuum chamber, shown in Fig. 1a. The pump and SC are focused using a lens with a focal length of 40 cm, entering the vacuum chamber through a 5 mm thick fused silica window and propagating 30 cm through vacuum to the target. The target is a copper gas flow tube with a flattened section through which a $120 \mu\text{m}$ diameter hole was laser drilled to allow the pump and probe to pass through. The space between the inner tube walls is 1 mm, with a wall thickness of 0.5 mm. A roots pump keeps the background pressure of the chamber at 400 mTorr, and the local gas density drops quickly enough away from the tube holes that the SSSI signal is dominated by the gas between the holes. The waist of the pump beam, measured by imaging the focus onto a CCD camera, is $22 \mu\text{m}$ FWHM. The pump beam is rejected at the exit of the vacuum chamber using a dichroic mirror that is also used as a window. In the data shown here, we have subtracted a very small background signal due to weak cross phase modulation in the entrance window.

The central plane of the gas tube is imaged onto the entrance slit of an imaging spectrometer. Because of the time delay between the probe and reference pulses, interference fringes appear in the spectrum. An example spectral interferogram using Ar at 60 TW/cm^2 vacuum intensity is shown in Fig. 1b. The pump pulse, centered at $t = t_{\text{pump}}$ and $x = x_{\text{pump}}$, causes a phase shift in the probe pulse $\Delta\phi(x, t)$. This is extracted in SSSI by measuring the change in spectral phase and amplitude of the probe beam [16]. The spectral phase is found by Fourier analysis of the interference fringes, and the change in amplitude is also found from the interferogram. The final piece of information required is the spectral phase of the reference pulse, which is, to an excellent approximation, quadratic and proportional to the GDD [16]. The extracted time domain phase shift $\Delta\phi(x, t)$ of the probe is shown in Fig. 1c. The phase shift is too small to produce fringe shifts visible by eye in Fig. 1b. The signal-to-noise ratio is considerably improved by summing multiple interferograms before performing the phase extraction [18]; in all of the data presented here, 300 interferograms were captured and summed at each power and polarization.

The optical nonlinearity in Ar is instantaneous to a very good approximation because the energy of the lowest electronic excitation is 15 eV, far greater than the photon energy 1.5 eV. Thus, we expect $\Delta\phi(x, t) \propto I_{\text{pump}}(x, t)$. The measured FWHM in Fig. 1c of 38 fs matches an autocorrelation measurement of the pump pulse. The spatial profile lineout, shown in Fig. 1d, agrees well with the pump spot profile. The deleterious effect of excessive interaction length on the width of the $\Delta\phi$ response is illustrated in Fig. 1d. A lineout of the measured phase shift along x at $t = t_{\text{pump}}$ is shown with the chamber backfilled with Ar – note the wider profile compared to the flow tube case. Also shown are simulations of the width of $\Delta\phi$ using the beam propagation method (BPM)

[19]; with the simulation we estimate the effective pump-gas interaction length as ~ 2 mm, in agreement with the tube geometry.

The ordinary Kerr effect is linear in the intensity: the refractive index is of the form $n = n_0 + n_2 I$, where n_0 is the index of refraction and n_2 is the Kerr coefficient. The peak phase shift measured in the experiment is plotted as a function of peak intensity in Fig. 1e. We find a very linear dependence for both Ar and N₂, and nearly the same Kerr coefficient, which is consistent with other experiments [20]. For the peak intensity I_{peak} of 60 TW/cm², Fig. 1c shows a peak phase shift in Ar of 0.059 radians. For a medium with an effective interaction length L_{eff} , $\Delta\phi_{\text{peak}} = 4\pi L_{\text{eff}} n_2 I_{\text{peak}} / \lambda$ (note the extra factor of 2 because we measure cross phase modulation). Using the literature value for Ar, $n_2 = 9.8 \times 10^{-20}$ cm²/W [20, 21] at 1 atm, and using $L_{\text{eff}} \approx 2$ mm, we estimate an average pressure in the interaction region of 0.3 atm. A higher-order Kerr effect would add terms of the form $n_{2m} I^m(t)$, where $m > 1$ [4]. No negative instantaneous phase is observed at any intensity in Ar or N₂, in disagreement with the $\Delta n(I)$ curve produced by Loriot *et al.* [4], nor do we see evidence of saturation [4, 15]. We have simulated the phase shift expected using the HOKE coefficients [4]; this is shown as a dashed line in Fig. 1e. The difference is stark and well outside any error in our experiment we can conceive of.

Increasing the pump intensity beyond the level of Fig. 1 requires careful consideration of increased SC generation by the pump itself, particularly when the pump polarization is parallel to the probe polarization. Because the pump and probe paths are not phase stable with respect to one another, spectral fringes between the pump supercontinuum and the reference pulse average out when many interferograms are summed. So the pump supercontinuum does not cause significant data distortion until it saturates the CCD camera, which occurs at intensities higher than 200 TW/cm², well beyond the ionization threshold of ~ 100 TW/cm² [22]. Maps showing $\Delta\phi(x, t)$ at high intensity in Ar are shown in Fig. 2. At high intensities we observe an additional response for $t > t_{\text{pump}}$ due to the plasma generated by ionization. The plasma produces a negative index contribution $\Delta n_{\text{plasma}} = -N_e / (2N_{cr})$, where N_e is the electron density and N_{cr} is the critical density. The plasma densities measured are consistent with calculations using Ammosov-Delone-Krainov (ADK) rates [23]. Plots of $\Delta\phi(x_{\text{pump}}, t)$ as a function of pump intensity are shown in Fig. 2c ($\mathbf{E}_{\text{pump}} \parallel \mathbf{E}_{\text{probe}}$) and Fig. 2d ($\mathbf{E}_{\text{pump}} \perp \mathbf{E}_{\text{probe}}$). Note that the plasma contribution seen in Fig. 2 is highly characteristic: (1) its onset at higher intensity (180 TW/cm² compared to 120 TW/cm²) eliminates the instantaneous Kerr response at the back of the pulse; the Kerr peak appears to move forward, (2) unlike the Kerr response, the plasma-induced phase shift is probe polarization independent, and (3) after generation, the plasma

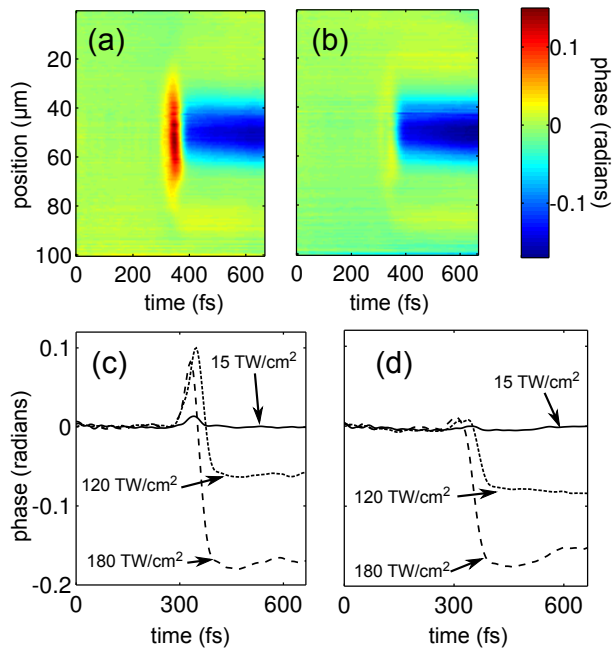


FIG. 2: (color online) Experimental data for Ar. (a,b) Maps of the extracted phase at 150 TW/cm² vacuum intensity, showing the positive electronic Kerr effect signal at $t = t_{\text{pump}}$ and the negative plasma signal at later time delays. (a) $\mathbf{E}_{\text{pump}} \parallel \mathbf{E}_{\text{probe}}$. (b) $\mathbf{E}_{\text{pump}} \perp \mathbf{E}_{\text{probe}}$. (c,d) Corresponding lineouts at the position of peak intensity as a function of pump intensity. Within error, the plasma response is constant in time after the pump has passed; we observe increased noise at the edges of the time window due to the decreased magnitude of the probe/reference SC on the spectral wings. The curves at 120 TW/cm² and 180 TW/cm² give electron densities $N_e = 7 \times 10^{15}$ cm⁻³ and $N_e = 2 \times 10^{16}$ cm⁻³ respectively.

response is long-lived on the time scale of this measurement, owing to recombination timescales of order ~ 100 ps.

In N₂, the optical Kerr response has an additional contribution from the transient alignment of the molecules in the strong optical field [24]. Results for N₂ are shown in Fig. 3; $\Delta\phi(x, t)$ is shown at low pump intensity for parallel and perpendicular polarization configurations in Fig. 3ab. The nonlinear index is $n(t) = n_2 I(t) + \int_0^\infty R(t') I(t - t') dt'$, where $R(t)$ is a response function that depends on properties of the rotational levels and the nuclear spin statistics [24, 25]. In nitrogen the rotational response peaks about 80 fs after the pulse arrives, as can be seen in Fig. 3a. Previous SSSI measurements [18, 25] were unable to resolve the two contributions, but here we can because of the shorter pump pulse. The ratio of the electronic Kerr effect for parallel to perpendicular polarization configurations is 3:1 in an isotropic medium. For the rotational component, the ratio is 2 : -1. The different symmetry properties allow the clean separation of the two contributions, as shown

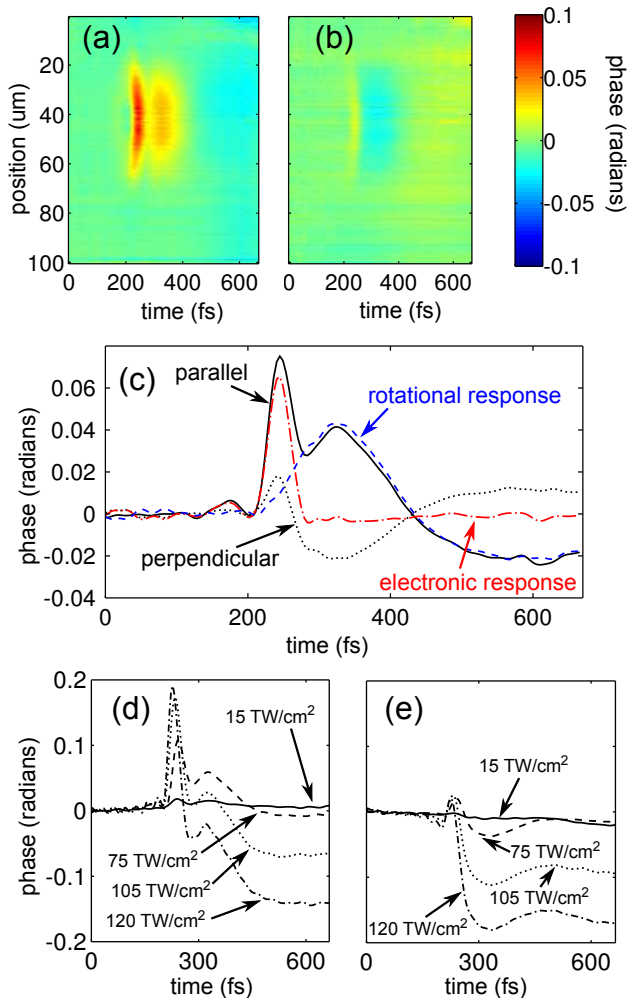


FIG. 3: (color online) Experimental data for N₂. (a,b) Maps of the extracted phase at 60 TW/cm² intensity, showing the positive instantaneous electronic Kerr effect (coincident with the pump), and the rotational response at later time delays. (a) $\mathbf{E}_{\text{pump}} \parallel \mathbf{E}_{\text{probe}}$. (b) $\mathbf{E}_{\text{pump}} \perp \mathbf{E}_{\text{probe}}$. (c) $\Delta\phi(x_{\text{pump}}, t)$ for the data shown in (a),(b). The decomposition of the signal into electronic and rotational components, as described in the text, is also shown. (d,e) Lineouts corresponding to (a,b) at the x_{pump} as a function of pump intensity.

in Fig. 3c. To our knowledge, these measurements are the first direct observation of the relative contributions of the electronic and rotational components of the Kerr effect in N₂. As with Ar, at higher intensities plasma is observed, as shown in plots of $\Delta\phi(x_{\text{pump}}, t)$ in Fig. 3de.

In summary, we have performed direct measurements of the optical Kerr effect in Ar and N₂ using single-shot supercontinuum spectral interferometry. In N₂, we are able to distinguish between electronic and rotational components of the nonlinearity, and the polarization dependence is consistent with theory. We observe the usual optical Kerr effect, linear in the intensity, as well as the onset of plasma, but no higher-order instantaneous

nonlinearities effecting either saturation or negative response. The fact that the pump-induced response appears to be linear in the intensity until the point of ionization is a reflection of the extremely nonlinear onset of ionization. At least for 40 fs pulses, there is no practical distinction between plasma and special atomic states with negative polarizability. These results constitute a definitive refutation of the idea that higher-order Kerr nonlinearities play an important role in filamentation in air [5]. Our results strongly confirm the long-standing conceptual picture [3] that short pulse filamentation in air arises from the dynamic balance between nonlinear self-focusing from bound electron nonlinearities and defocusing due to plasma generation.

J.K.W. thanks the Joint Quantum Institute for support. We thank Y.-H. Chen and S. Varma for helpful discussions. This research was supported by the National Science Foundation, the U.S. Department of Energy, the Office of Naval Research, and the Lockheed-Martin Corporation.

-
- [1] G. P. Agrawal, *Nonlinear Fiber Optics* (Academic Press, 2006), 4th ed.
 - [2] H. A. Haus, *IEEE. J. Sel. Topics Quantum Electron.* **6**, 1173 (2000).
 - [3] A. Couairon and A. Mysyrowicz, *Phys. Rep.* **441**, 47 (2007).
 - [4] V. Loriot, E. Hertz, O. Faucher, and B. Lavorel, *Opt. Express* **17**, 13429 (2009).
 - [5] P. B ejot, J. Kasparian, S. Henin, V. Loriot, T. Vieillard, E. Hertz, O. Faucher, B. Lavorel, and J.-P. Wolf, *Phys. Rev. Lett.* **104**, 103903 (2010).
 - [6] D. Novoa, H. Michinel, and D. Tommasini, *Phys. Rev. Lett.* **105**, 203904 (2010).
 - [7] Y.-H. Chen, S. Varma, T. M. Antonsen, and H. M. Milchberg, *Phys. Rev. Lett.* **105**, 215005 (2010).
 - [8] O. Kosareva, J. Daigle, N. Panov, T. Wang, S. Hosseini, S. Yuan, G. Roy, V. Makarov, and S. L. Chin, *Opt. Lett.* **36**, 1035 (2011).
 - [9] P. Polynkin, M. Kolesik, E. M. Wright, and J. V. Moloney, *Phys. Rev. Lett.* **106**, 153902 (2011).
 - [10] M. Kolesik, D. Mirell, J. Diels, and J. V. Moloney, *Opt. Lett.* **35**, 3685 (2010).
 - [11] P. B ejot, E. Hertz, J. Kasparian, B. Lavorel, J.-P. Wolf, and O. Faucher, *Phys. Rev. Lett.* (accepted, 2011).
 - [12] M. Kolesik, E. M. Wright, and J. V. Moloney, *Opt. Lett.* **35**, 2550 (2010).
 - [13] P. B ejot, E. Hertz, B. Lavorel, J. Kasparian, J.-P. Wolf, and O. Faucher, *Opt. Lett.* **36**, 828 (2011).
 - [14] A. Teleki, E. M. Wright, and M. Kolesik, *Phys. Rev. A* **82**, 065801 (2010).
 - [15] C. Br ee, A. Demircan, and G. Steinmeyer, *Phys. Rev. Lett.* **106**, 183902 (2011).
 - [16] K. Y. Kim, I. Alexeev, and H. M. Milchberg, *Appl. Phys. Lett.* **81**, 4124 (2002).
 - [17] Going from a measurement of the transient birefringence to Kerr coefficients requires careful accounting of all relevant tensor components, as discussed in G. Stegeman,

- D. G. Papazoglou, R. Boyd, and S. Tzortzakis, *Opt. Express* **19**, 6387 (2011).
- [18] Y.-H. Chen, S. Varma, I. Alexeev, and H. Milchberg, *Opt. Express* **15**, 7458 (2007).
- [19] The distorting effects of using an interaction length in spectral interferometry much longer than the Rayleigh range are discussed and simulated in K. Y. Kim, I. Alexeev, and H. M. Milchberg, *Opt. Express* **10**, 1563 (2002).
- [20] C. Marceau, S. Ramakrishna, S. Génier, T. Wang, Y. Chen, F. Théberge, M. Châteauneuf, J. Dubois, T. Seideman, and S. L. Chin, *Opt. Commun.* **283**, 2732 (2010).
- [21] H. Lehmeier, W. Leupacher, and A. Penzkofer, *Opt. Commun.* **56**, 67 (1985).
- [22] S. Augst, A. Talebpour, S. L. Chin, Y. Beaudoin, and M. Chaker, *Phys. Rev. A* **52**, R917 (1995).
- [23] M. V. Ammosov, N. B. Delone and V. P. Krainov. *Sov. Phys. JETP* **64**, 1191 (1986).
- [24] E. T. J. Nibbering, G. Grillon, M. A. Franco, B. S. Prade, and A. Mysyrowicz, *J. Opt. Soc. Am. B* **14**, 650 (1997).
- [25] Y.-H. Chen, S. Varma, A. York, and H. M. Milchberg, *Opt. Express* **15**, 11341 (2007).